Figure 2.

PS-SKS splitting for receiver side anisotropy only

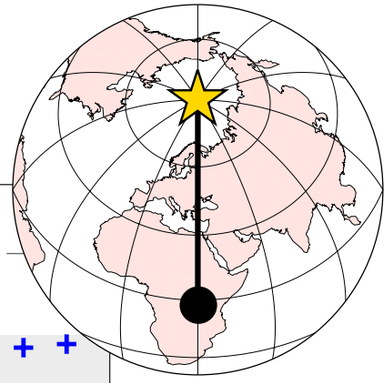

(a) Olivine A-type

(b) Olivine C-type

(c) Olivine E-type

Splitting intensity

Rotation Angle / °

SKS PS abs(SI(PS-SKS))

Influence of SP phase

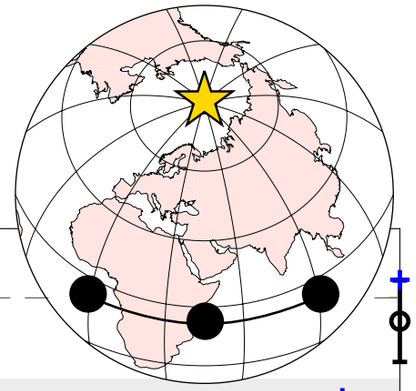

(d) Strike-slip fault

(e) Normal fault

Splitting intensity

Backazimuth / °

Figure 3.

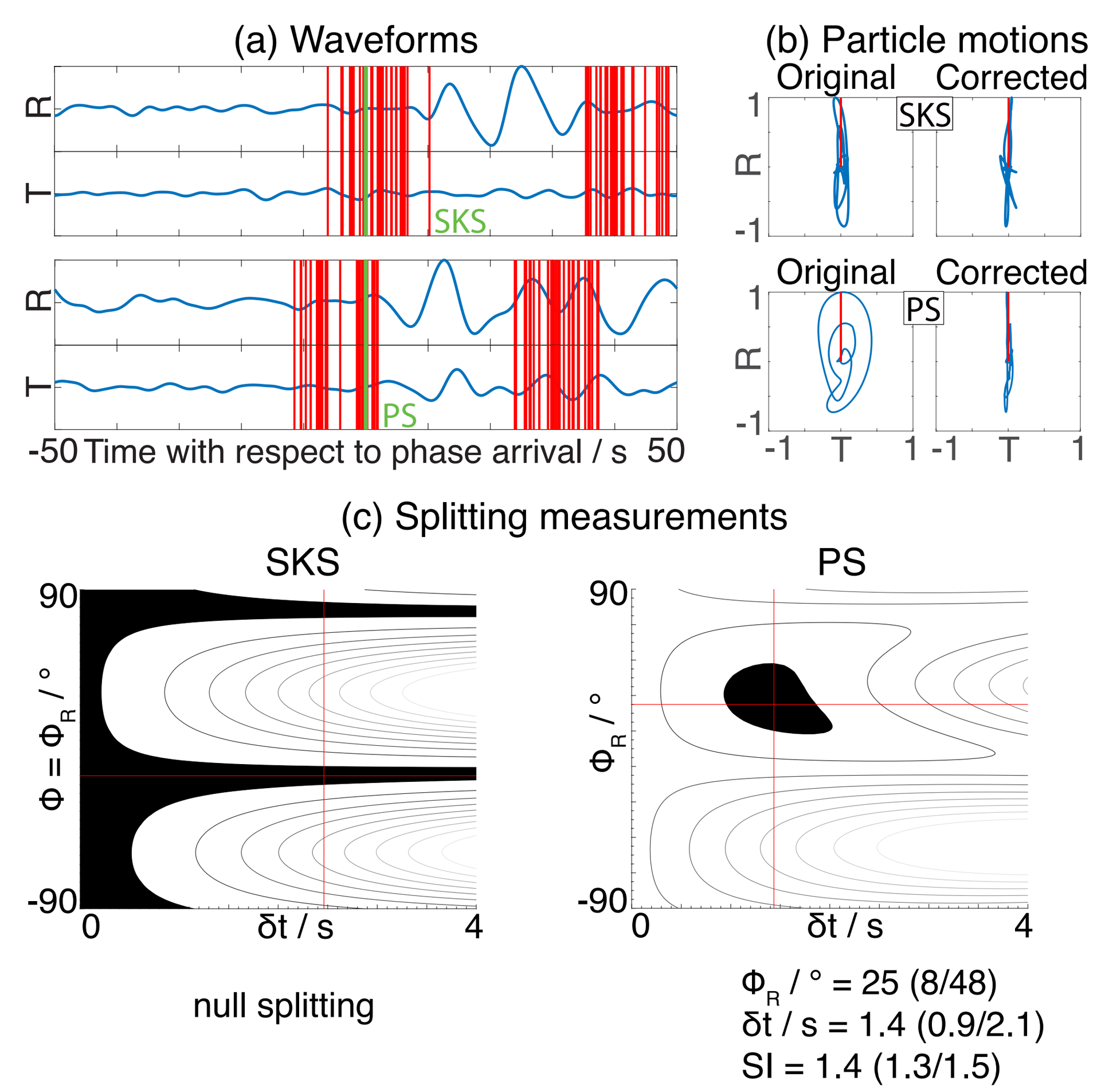
(a) Waveforms
R
T
SKS
R
T
PS
-50
Time with respect to phase arrival / s
50
(b) Particle motions
Original
Corrected
SKS
R
1
-1
Original
Corrected
PS
R
1
-1
-1
T
1
-1
T
1
(c) Splitting measurements
SKS
90
Φ = Φ_R / °
-90
0
δt / s
4
PS
90
Φ_R / °
-90
0
δt / s
4
null splitting
Φ_R / ° = 25 (8/48)
δt / s = 1.4 (0.9/2.1)
SI = 1.4 (1.3/1.5)

Figure 1.

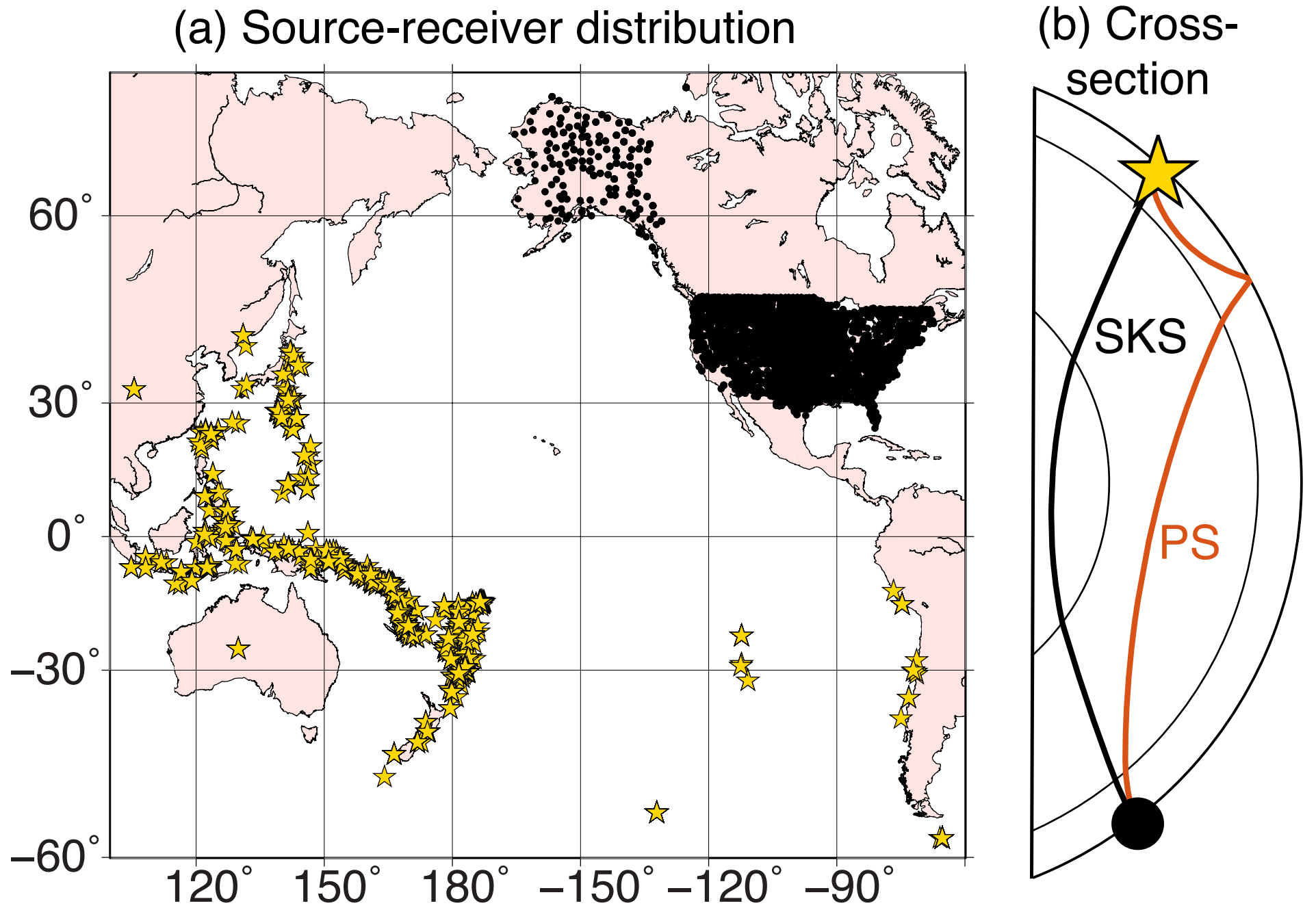
(a) Source-receiver distribution
60°
30°
0°
−30°
−60°
120°
150°
180°
−150°
−120°
−90°
(b) Cross-section
SKS
PS

Figure 5.

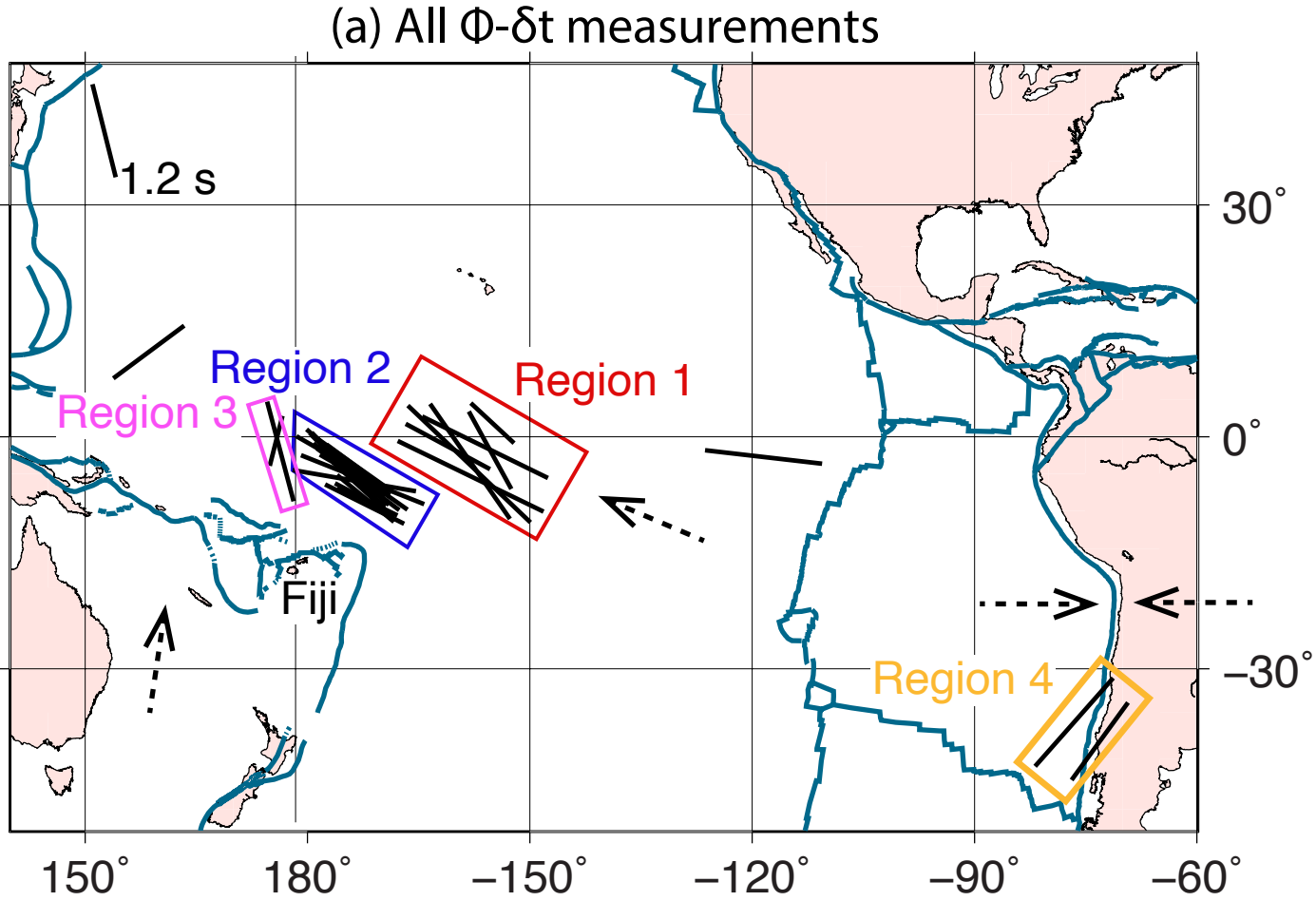
(a) All Φ-δt measurements
1.2 s
Region 1
Region 2
Region 3
Region 4
Fiji
30˚
0˚
–30˚
150˚
180˚
–150˚
–120˚
–90˚
–60˚

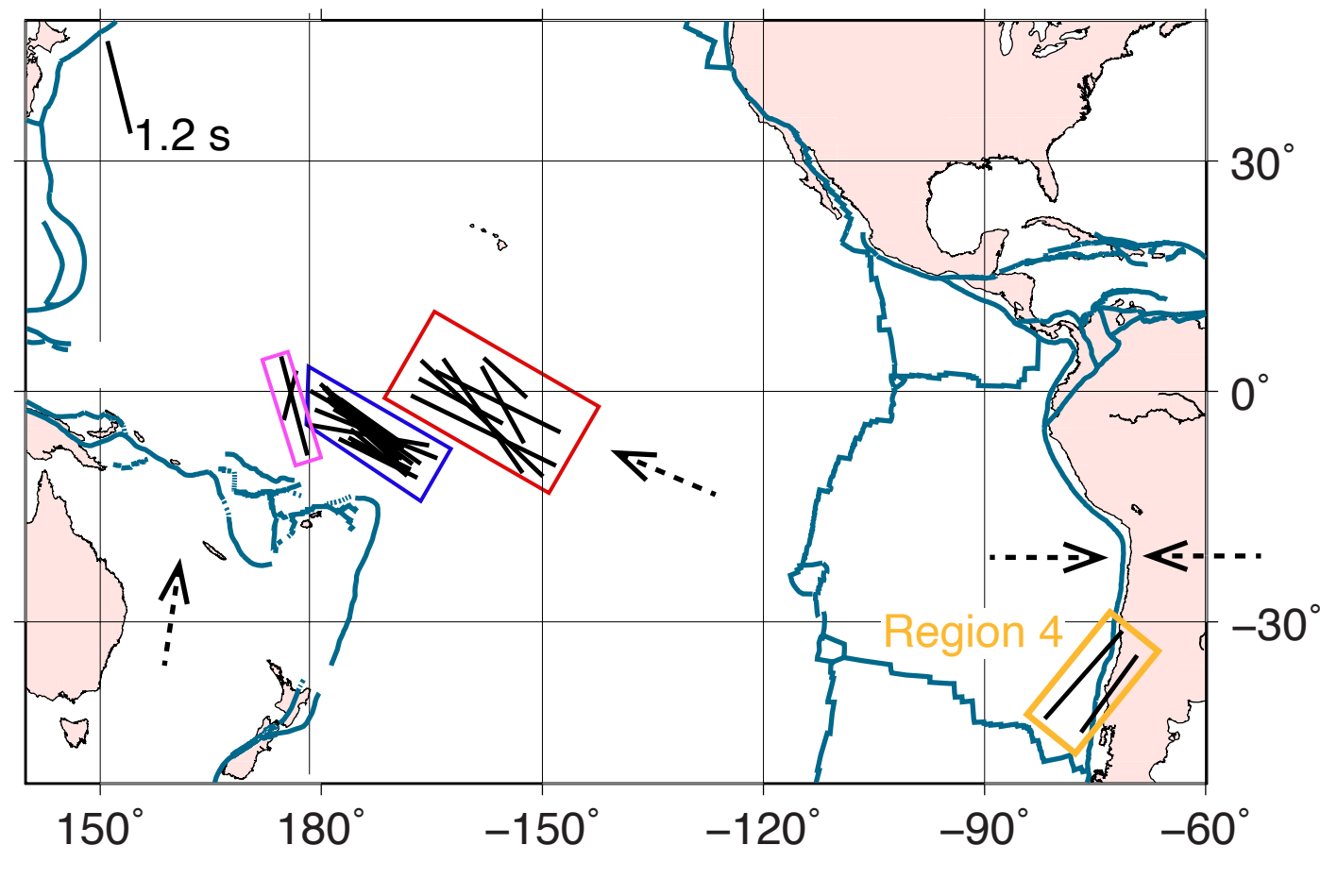
1.2 s
30˚
0˚
–30˚
Region 4
150˚
180˚
–150˚
–120˚
–90˚
–60˚

Figure 4.

(a)

A

B

C

D

E

F

Fiji

0.0 0.7

δ(SI)

(b)

0 >200

Rays per bin

30˚

0˚

–30˚

(c)

Fiji

120˚ 150˚ 180˚ –150˚ –120˚ –90˚

(d)

0 >60

Rays per bin

30˚

0˚

–30˚

120˚ 150˚ 180˚ –150˚ –120˚ –90˚

Upper mantle anisotropy and flow beneath the Pacific Ocean revealed by differential PS-SKS splitting

Jonathan Wolf[1], **Maureen D. Long**[1]

[1]Department of Earth and Planetary Sciences, Yale University, New Haven, CT, USA

Key Points:

- We infer seismic anisotropy beneath the Pacific Ocean from differential PS-SKS shear-wave splitting.
- A majority of our measurements can be explained by plate motion induced shearing.
- Far-field effects of subduction-induced, three-dimensional flow lead to a rotation of fast directions in the upper mantle north of Fiji.

Corresponding author: Jonathan Wolf, jonathan.wolf@yale.edu

Abstract

Upper mantle anisotropy has been mapped beneath continents at high spatial resolution. Beneath the oceans, however, shear wave splitting constraints on upper mantle anisotropy are sparse, due to the paucity of seismic receivers. The technique that does not require the availability of seismic stations close to the region under study is differential PS-SKS splitting. Here, we use global wavefield simulations to investigate circumstances under which PS-SKS splitting can be applied, and then use this technique to measure upper mantle anisotropy beneath the Pacific Ocean basin. Our results demonstrate that upper mantle anisotropy in our study region mostly reflects shearing due to the Pacific plate. North of Fiji, we observe a rotation of fast polarization directions, away from the direction of absolute plate motion of the Pacific plate. We attribute this to far-field mantle flow effects associated with the subduction of the Australian plate beneath the Pacific.

Plain Language Summary

Earthquakes cause seismic waves whose speeds sometimes depend on their propagation direction. This material property, called seismic anisotropy, can be used to infer the direction of flow in Earth's upper mantle. Seismic anisotropy is straightforward to measure directly beneath a seismic station, but harder to study if station coverage is sparse. We use a technique that allows us to infer upper mantle seismic anisotropy beneath the Pacific Ocean in places without nearby seismic stations. Our measurements show that while seismic anisotropy varies laterally beneath the Pacific Ocean, in most cases it can be explained by the movement of the Pacific tectonic plate, leading to deformation in the underlying mantle. North of Fiji, we can observe the effects that the subduction of the Australian beneath the Pacific tectonic plate has on upper mantle flow.

1 Introduction

Seismic anisotropy, or the dependence of seismic wavespeeds on polarization or propagation direction of the wave, has been extensively studied in the upper mantle (e.g., Silver, 1996; Savage, 1999; Liu et al., 2014; Zhu et al., 2020). It can be characterized using surface waves, which permit a relatively good depth resolution of seismic anisotropy (e.g., Yu & Park, 1993; Panning & Nolet, 2008; Yuan & Beghein, 2014); alternatively, shear-wave splitting of body waves can be used for a higher lateral resolution (e.g., Russo et al., 2010; Walpole et al., 2014; Lopes et al., 2020; Wolf et al., 2023). The typical motivation to study seismic anisotropy is to map man-

tle deformation and flow (e.g., Karato et al., 2008). The fast polarization direction of upper mantle anisotropy often aligns with plate motions (e.g., Silver, 1996; Long & Becker, 2010; Becker & Lebedev, 2021), although there are some exceptions, particularly in subduction zones (e.g., Kneller et al., 2005; Karato et al., 2008; Long, 2013). Therefore, measurements of upper mantle seismic anisotropy are a powerful tool to map the global upper mantle flow field.

Measurements of shear-wave splitting are commonly applied to SKS, SKKS and PKS (*KS) phases and are generally thought to mainly reflect seismic anisotropy in the upper mantle beneath the station (e.g., Silver, 1996; Liu et al., 2014; Walpole et al., 2014), although contributions from the lowermost mantle are possible (e.g., Niu & Perez, 2004; Lynner & Long, 2012; Wolf et al., 2019; Wolf & Long, 2022). *KS are popular target phases because they are initially radially polarized due to the P to SV conversion at the core-mantle boundary (CMB). Splitting measurements from *KS phases have been applied to a large number of stations across the globe, and many measurements have been made available in open access databases (e.g., Barruol et al., 2009; Trabant et al., 2012; Liu et al., 2014). These databases give an excellent overview about upper mantle splitting world-wide, although there are some poorly sampled areas. The abundance of splitting data is controlled by the station density in any particular region. For example, data coverage is sparse beneath ocean basins (e.g., Barruol et al., 2009; Trabant et al., 2012; Liu et al., 2014) because seismic receivers are difficult and expensive to install there.

Su and Park (1994) suggested that the global resolution of upper mantle anisotropy can be improved by comparing shear-wave splitting of PS and SKS phases (Figure 1b), a method that has not been used since. PS and SKS are both initially SV polarized before sampling anisotropy due to the P-SV conversions along their raypaths. They both sample similar upper mantle anisotropy beneath the receiver; however, PS additionally accumulates splitting on the portion of its raypath that travels through upper mantle anisotropy after bouncing off the surface. Therefore, differential splitting of PS and SKS for the same station-event pair indicates an upper mantle anisotropy contribution close to the PS bounce point. If seismic stations are available in the vicinity of the PS bounce point, then there is no clear advantage of using PS-SKS splitting instead of traditional SKS splitting measurements. However, if no seismic stations are available, then PS-SKS splitting is an excellent option. Thus, PS-SKS splitting holds potential to fill in sampling gaps of upper mantle anisotropy studies, particularly beneath ocean basins.

In this study, we analyze upper mantle anisotropy beneath the Pacific Ocean, which has only been sparsely sampled to date using shear wave splitting measurements (e.g., Barruol et al., 2009; Trabant et al., 2012; Liu et al., 2014). We apply the PS-SKS splitting technique to events in with moment magnitudes > 6.0 that occurred between 01/2006 and 12/2022 in an epicentral distance of 90° to 115° from USArray (IRIS Transportable Array, 2003) stations, in the continental United States and Alaska. This allows us to construct a large dataset (consisting of 320,000 seismograms in total; Figure 1a). We show that fast polarization directions of upper mantle anisotropy tend to align with the absolute plate motion of the Pacific plate for much of our study region. In the southern part of our study region we can observe a rotation of fast polarization directions, likely caused by far-field effects on upper mantle flow by the Vanuatu subduction zone.

2 Shear-wave splitting measurements

When a shear wave travels through an anisotropic medium, it splits into two components, one traveling relatively slow and the other traveling fast. The time delay between these two components is usually referred to as δt, while the polarization direction of the fast travelling wave (measured clockwise to the north) is called ϕ. We call the fast polarization direction measured at the station ϕ_R. This parameter, translated to the bounce point reference frame for PS, can be expressed via $\phi = b - (\phi_R - b)$, with b denoting the backazimuth. A parameter that can be used to define the strength of splitting for a given seismogram is the splitting intensity (Chevrot, 2000), SI, defined as

$$SI = -2\frac{T(t)R'(t)}{|R'(t)|^2} \approx \delta t \sin(2(b-\phi_R)) \tag{1}$$

where R(t) is the radial component, $R'(t)$ is the time derivative of the radial component and $T(t)$ is the transverse component. The splitting intensity is large if the transverse component, $T(t)$, and the radial component time derivative, $R'(t)$, have a similar waveform shape, and if the amplitude of the transverse component is large, reflecting energy that has been partitioned from the radial to the transverse component.

We use SplitRacer_auto (Reiss & Rümpker, 2017; Link et al., 2022) to automatically measure the splitting parameters (ϕ, δt and SI) for our large PS-SKS dataset. We filter our data retaining periods between 6 and 25 s. Then, we calculate splitting parameters for 30 randomly selected time windows, and only retain measurements if they are largely independent of the measurement window. SplitRacer_auto uses the transverse component minimization tech-

nique (Silver & Chan, 1991), and calculates 95% confidence intervals using the corrected algorithm of Walsh et al. (2013). We modify SplitRacer_auto slightly to be able to make splitting measurements for PS phases.

3 PS-SKS splitting: Method verification

At an epicentral distance of ~90°, SKS starts to be clearly separated from S and ScS. The PS turning point in the mantle is more than 500 km above the core-mantle boundary for epicentral distances < 115°, such that no major contribution from deep mantle anisotropy (typically confined to D″ layer; e.g., Panning and Romanowicz (2006)) can be expected to influence PS at these distances. We therefore choose to investigate PS-SKS splitting in the epicentral distance range between 90 and 115°.

Before we can apply the PS-SKS splitting technique systematically, however, we explore two possible sources of uncertainty. First, while the raypaths of PS and SKS are similar in the upper mantle beneath the receiver, they are not completely identical (Figure 1b). We therefore investigate the threshold difference in PS and SKS splitting for which differential splitting is robustly indicative of anisotropy close to the PS bounce point. Second, we investigate whether SP, which arrives mainly on the vertical component but at the same time as PS for a focal depth of 0 km, does influence the measured PS splitting parameters. To explore these two questions we use global wavefield simulations with AxiSEM3D (Leng et al., 2016, 2019), following previous work (Tesoniero et al., 2020; Wolf et al., 2022b, 2023).

For our simulations we always place the source at the North Pole, simulating an earthquake with either 0 km or 500 km focal depth. The background velocity structure in our simulations is always isotropic PREM (Dziewonski & Anderson, 1981), which is replaced at certain depths in the upper mantle by seismic anisotropy. To describe the seismic anisotropy, we use the olivine elastic tensors from Table 21.1. in Karato (2008) for the fabric types that are potentially widespread in the upper mantle (A, C, and E), assuming a horizontal simple shear configuration. We incorporate these elastic tensors starting at a depth of 24 km and then adjust the anisotropic layer thickness such that the maximum (sampling azimuth dependent) delay time (depending on the sampling azimuth) is ~1 s.

In the first set of simulations we investigate the maximum difference in PS and SKS splitting for an anisotropic layer beneath the receiver and no seismic anisotropy at the bounce point. To test this, we conduct simulations for an epicentral distance of 90° (Figure 2a inset), for which

the spatial separation of PS and SKS raypaths in the upper mantle beneath the receiver is the largest. We simulate an earthquake at 500 km depth, whose focal mechanism is chosen to maximize PS and SKS amplitudes by yielding an initially fully radially polarized S wave, with M_{tt} as the only non-zero component of the moment tensor. We rotate the A-, C- and E-type elastic tensors around the vertical axis in increments of 15°, thus sampling different portions of the tensor with propagating PS and SKS waves, and measure PS and SKS splitting intensities (Figure 2a-c). We find that while the detailed patterns depend on the fabric type, upper mantle anisotropy beneath the receiver can account for SI differences up to 0.4 between PS and SKS (Figure 2a-c). Splitting intensities of PS and SKS phases are more similar for olivine E-type (Figure 2c) than A- and C-type (Figure 2a,b).

To test whether the contemporaneous SP arrival influences the measured PS splitting parameters, we conduct a second set of simulations. We simulate a strike-slip and a normal faulting event with a focal depth of 0 km at the North Pole and place stations at an epicentral distance of 100°, spaced every 5° in longitude (Figure 2d-e inset). We measure PS-SKS splitting for waves arriving from backazimuths from 0° to 90°. This measures energy from one quadrant of the moment tensor, thereby effectively varying PS/SP amplitudes as a function of backazimuth. For all simulations, we incorporate the same olivine A-type elastic tensor in the upper mantle, such that splitting parameters should be independent of backazimuth. For the strike-slip event, for backazimuths around 0° and 90°, due to the radiation pattern, there is little initial SV energy; in practice such seismograms would be discarded in the pre-processing (Figure 2d). Apart from that, for both the strike-slip (Figure 2d) and the normal fault event (Figure 2e), PS splitting intensities are essentially the same regardless of backazimuth. Thus, we infer that the influence of different PS-SP amplitudes on PS splitting measurements is negligible, and SP cannot be expected to interfere substantially with PS splitting measurements.

Summarizing our modeling results, we have shown that PS-SKS splitting intensity differences greater than ~0.4 can likely be attributed to anisotropy near the PS bounce point. This 0.4 cutoff is chosen considering a worst-case scenario with an epicentral distance of 90° (Figure 2). Additionally, we have demonstrated that SP does not interfere strongly with PS splitting, which enables us to measure PS-SKS splitting for any focal depth.

4 Results

We obtain ~6000 PS-SKS pairs for which both phases have well-constrained splitting intensities, which we define as having a maximum size of the 95% confidence interval of ±0.3. We additionally obtain 35 splitting measurements for which SKS splitting is null ($|SI| < 0.3$) and ϕ-δt-measurements for PS are well-constrained. We consider PS (ϕ, δt) measurements well-constrained whenever the size of the 95% confidence intervals is smaller than ±25° for ϕ and ±0.8 s for δt. A splitting measurement example for such a PS-SKS pair is shown in Figure 3. In this case, the SKS transverse component energy is close to the noise level, suggesting null or near-null splitting; in contrast, we can observe clear PS splitting. Since SKS splitting is null, PS splitting can mainly be attributed to bounce point anisotropy. Besides the splitting intensity, for this example ϕ and δt are also well-constrained for PS, revealing the fast polarization direction and time delay associated with upper mantle anisotropy near the bounce point.

We first focus on spatial patterns of differential PS-SKS splitting intensity discrepancies. In general, splitting intensity discrepancies will depend on the sampling direction of the anisotropy, as well as on the strength and geometry of anisotropy. However, since all data sample the upper mantle from a similar direction in any particular region in our dataset, it is useful to average our differential splitting intensity measurements in spatial bins, since individual data points (plotted at the PS bounce point) lie on top of each other. We bin our data using two different bin sizes, 5° × 5° and 2.5° × 2.5°; the results are shown in Figure 4. Overall, we can identify six distinct anisotropic regions, labeled A-F in Figure 4a. For the identification of these regions we only focus on clusters of bins that indicate strong PS-SKS splitting discrepancies (Figure 4a,c), and only select those bins that exhibit a good ray coverage (Figure 4b,d) with more than 10 measurements per bin. The distribution of those regions illustrates that the upper mantle beneath the Pacific Ocean is anisotropic in many areas. We emphasize that with our approach, we are not able to exclude the possibility of upper mantle anisotropy in regions that do not exhibit large PS-SKS splitting discrepancies. While the absence of seismic anisotropy is one explanation for low PS-SKS splitting intensity discrepancies, another explanation is that the upper mantle seismic anisotropy close to the PS bounce point is sampled from a direction that does not lead to strong PS splitting (that is, a null direction).

More informative than the differential PS-SKS splitting intensities are measurements of fast polarization directions and delay times caused by upper mantle anisotropy close to the

PS bounce point. To avoid applying explicit ray-theoretical corrections for receiver side upper mantle anisotropy, which can have significant uncertainties (Wolf et al., 2022a), we focus on PS-SKS pairs for which SKS splitting is null and (ϕ-δt) measurements for PS are well-constrained. There are four different anisotropic regions for which we obtain well constrained ϕ-δt-measurements for more than one PS wave (Figure 5a). Fast polarization directions are oriented roughly east-southeast/west-northwest for regions 1 and 2 (Figure 5a); average delay times are approximately 30% larger for region 2. For region 3, which is located just to the west of region 2, fast polarization directions are oriented almost south/north. Region 4 shows southwest-northeast fast polarizations orientations. The other measurements are scattered across different locations and generally show no consistent orientation of fast polarization directions.

5 Discussion

No traditional SKS splitting measurements are available in our study region in global databases. Measurements made using ocean bottom seismometer (Takeo et al., 2016) data and on ocean island stations (Fontaine et al., 2007) around French Polynesia, to the south and east of regions 1 and 2 (Figure 5), show fast polarization directions that generally align with the absolute plate motion direction of the Pacific plate. Previous PS-SKS splitting results from Su and Park (1994) focused on a region slightly to the south of region 2, and agree with the fast polarization directions measured in this study. Additionally, patterns of azimuthal anisotropy at ~200 km depth that have been inferred from surface waves in multiple studies (e.g., Lebedev & Van Der Hilst, 2008; Becker, 2012; Yuan & Beghein, 2014; Debayle et al., 2016; Eddy et al., 2022) are similar to our measurements in regions 1 and 2. Taken together, our results and the results from previous studies suggest consistent east-southeast oriented fast directions in and around regions 1 and 2. These fast polarization directions agree well with the direction of absolute plate motion of the Pacific plate (Figure 5), and are therefore likely primarily caused by plate motion induced shearing in the asthenospheric upper mantle.

To the east of region 1, in region 3, we can observe a rotation of fast polarization directions to being nearly south-north (Figure 5) which is close to the propagation direction of the PS waves in our dataset. A more nearly North-South fast direction in this region would explain the low splitting intensities to the east of regions C and D in Figure 4; these are consistent with a that the fast polarization direction of upper mantle anisotropy that is approximately parallel to the propagation direction of the wave. This geometry is generally consistent with azimuthal anisotropy models derived from surface waves (e.g., Yuan & Beghein, 2014; Eddy et

al., 2022), which show weak anisotropy in this region for depths > 100 km and approximately north-northeast fast polarization directions above that depth. In fact, measurements of azimuthal anisotropy from surface waves show fast polarization directions that differ from the direction of absolute plate motion in regions adjacent circum-Pacific subduction zones (e.g., Yuan & Beghein, 2014; Eddy et al., 2022). We hypothesize that the rotation of fast polarization directions in region 3 is likely caused by far-field effects of three dimensional flow associated with the subduction of the Australian underneath the Pacific plate (Faccenda & Capitanio, 2012; Paczkowski et al., 2014).

As in the other regions, published SKS splitting results are not available in global databases for region 4. We compare our measured fast polarization directions to surface-wave derived azimuthal anisotropy, and find they agree well at depths < 200 km (e.g., Yuan & Beghein, 2014; Eddy et al., 2022). This direction is not parallel to the absolute motion of the Nazca plate; rather it is nearly parallel to oblique to the trench of the south American subduction zone. This direction may indicate a component of three-dimensional flow in the South American subduction system, consistent with inferences from elsewhere along the margin (e.g., Eakin et al., 2014; Long et al., 2016; Lynner & Beck, 2020)

6 Conclusion

We used the PS-SKS splitting technique to measure upper mantle anisotropy beneath the Pacific Ocean, a region in which splitting measurements using traditional *KS splitting techniques are hard to obtain due to a paucity of seismic stations. Our results indicate that seismic anisotropy is mostly caused by shear associated with the motion of the Pacific plate. Close to Nauru we observe a rotation of upper mantle fast polarization directions north of Fiji, likely caused by three dimensional flow associated with the Vanuatu subduction zone.

Data and code availability

All USArray data (IRIS Transportable Array, 2003) are publicly available at IRIS (`https://service.iris.edu/`). The synthetic seismograms for this study were computed using AxiSEM3D which is publicly available at `https://github.com/AxiSEMunity` (Leng et al., 2016, 2019).

Acknowledgments

This work was funded by Yale University. We thank the Yale Center for Research Computing for providing the necessary research computing infrastructure for this study. The Generic Mapping Tools (Wessel & Smith, 1998) and ObsPy (Beyreuther et al., 2010) were used in this research.

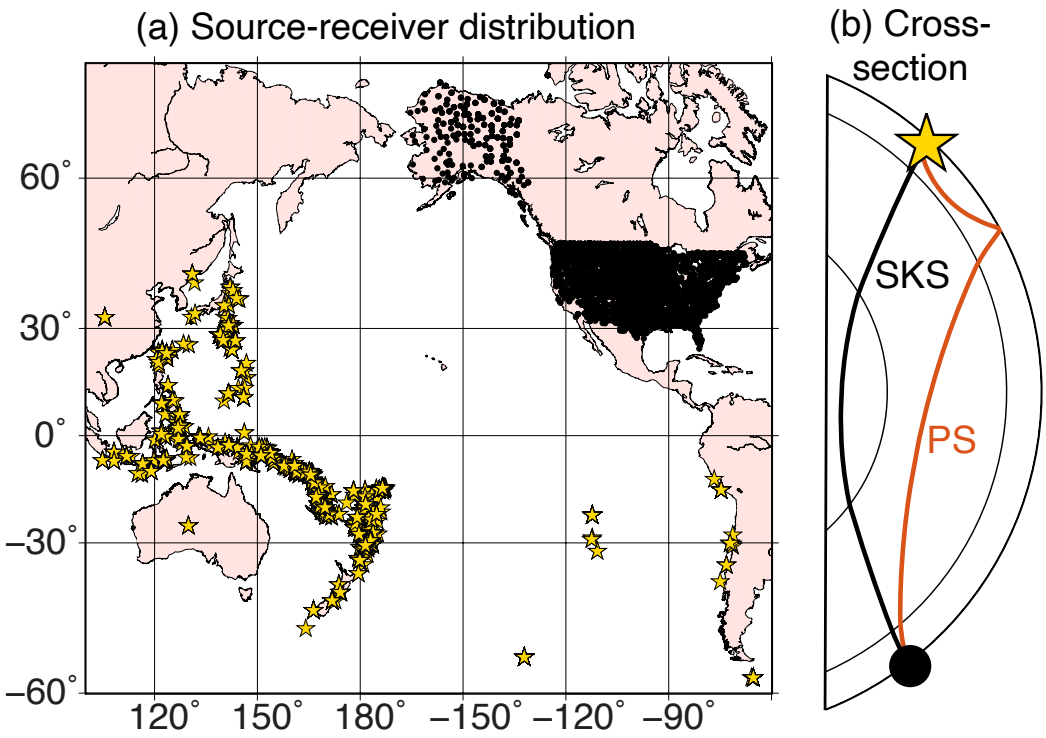

Figure 1: (a) Source-receiver distribution for all event-station pairs for which at least one well-constrained differential PS-SKS splitting intensity measurement could be obtained. Events are represented as yellow stars and stations as black circles. (b) Cross-section showing SKS (black) and PS (red) raypaths for an epicentral distance of 110°.

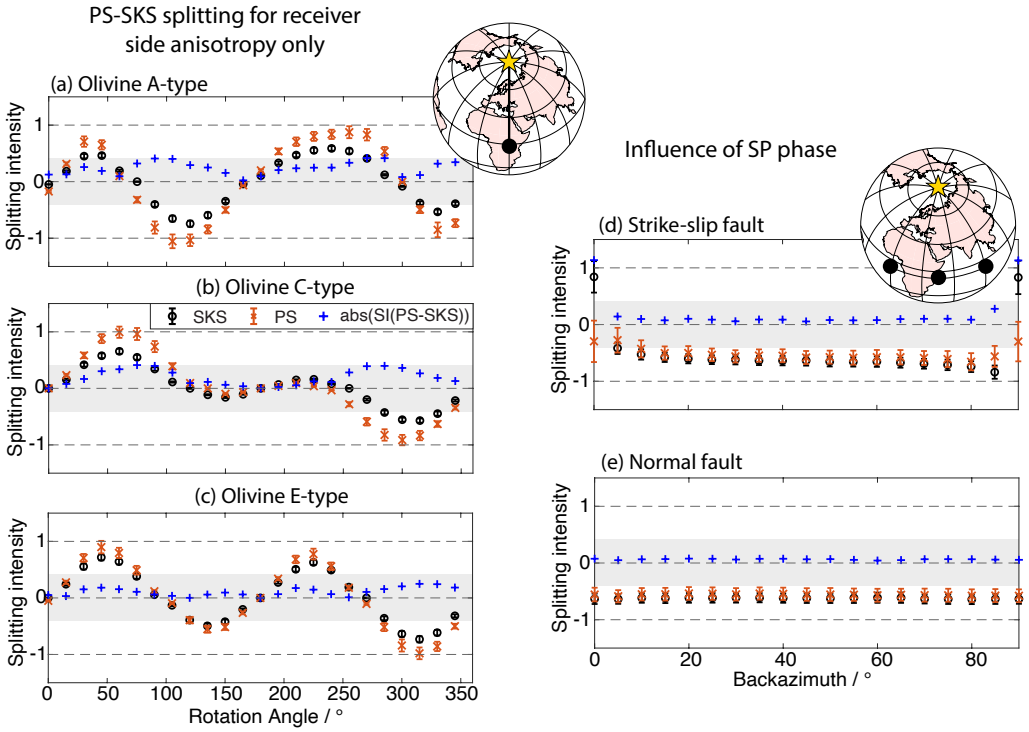

Figure 2: Results from global wavefield simulations that investigate (a-c) PS-SKS splitting in the presence of (only) receiver side anisotropy and (d-e) the influence of the SP phase on splitting parameters. (a) PS (red) and SKS (black) splitting intensities along with their absolute differences (blue) as a function of rotation angle (in the horizontal plane) of an olivine A-type elastic tensor (see text). The source-receiver configuration is shown on the inset. Gray shading indicates splitting intensities between -0.4 and 0.4. (b) Same as (a) for an olivine C-type elastic tensor. (c) Same as (a) for an olivine E-type elastic tensor. (d) PS (red) and SKS (black) splitting intensities and their absolute differences (blue) as a function of backazimuth for an olivine A-type elastic tensor and a strike-slip event. Other plotting conventions are as in panel (a). (e) Same as panel (d) for a normal fault event.

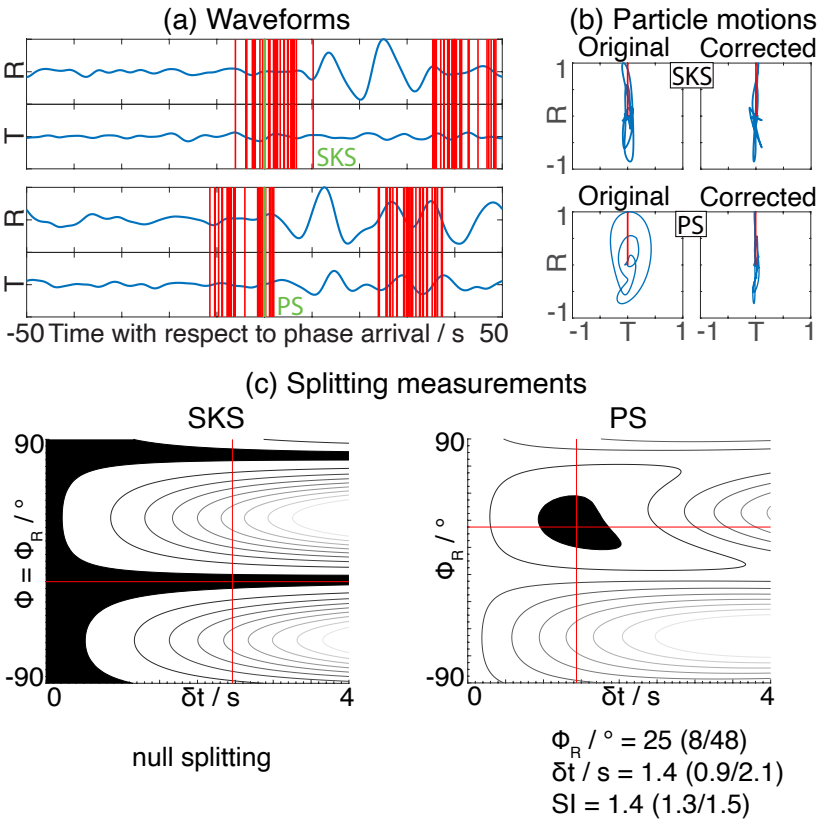

Figure 3: Differential PS-SKS splitting measured at station Q31A for an event that occurred 08/10/2010 (moment magnitude: 7.3; focal depth: 34 km). (a) SKS (top) and PS (bottom) radial (R) and transverse (T) waveforms. The PREM-predicted phase arrival time is shown by a green line and the start/end of the automatically selected measurement windows are shown as red lines. SKS transverse energy is at the noise amplitude level; therefore, SKS splitting is null. (b) PS particle motions before (left) and after (right) correcting for the phase's best fitting splitting parameters. Both are linear for SKS whose splitting is null (top), while only the corrected particle motion of the split PS phase is linear (bottom). (c) Best fitting splitting parameters for SKS (left) and PS (right) in the ϕ_R-δt plane. The 95% confidence interval is shown in black. SKS splitting is null, while ϕ, δt and SI, given by the values at lower right, are well-constrained for PS.

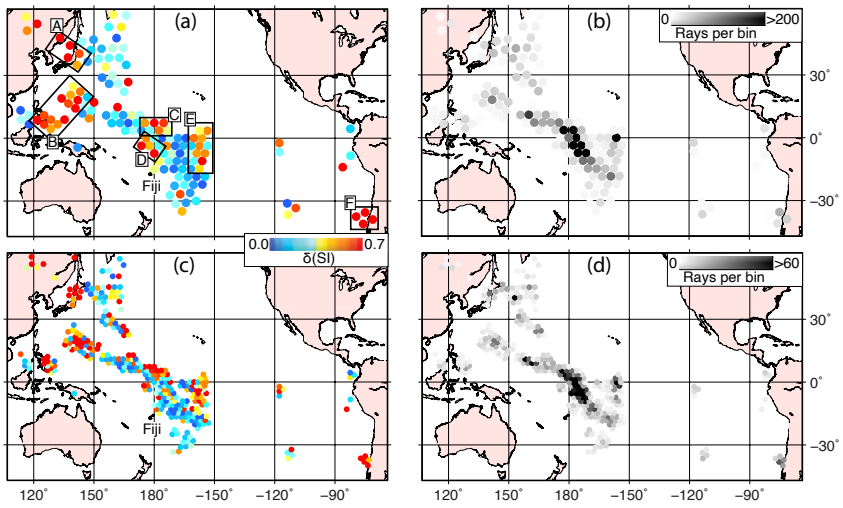

Figure 4: Average PS-SKS splitting intensity discrepancies plotted at the PS bounce point and binned spatially (δSI, see legend; panels a,c), along with the number of measurements per bin (see legend; panels b,d) for bin sizes of $5^\circ \times 5^\circ$ (a,b) and $2.5^\circ \times 2.5^\circ$ (c,d). Distinct regions (A-F) with high splitting intensity discrepancies are marked in panel a.

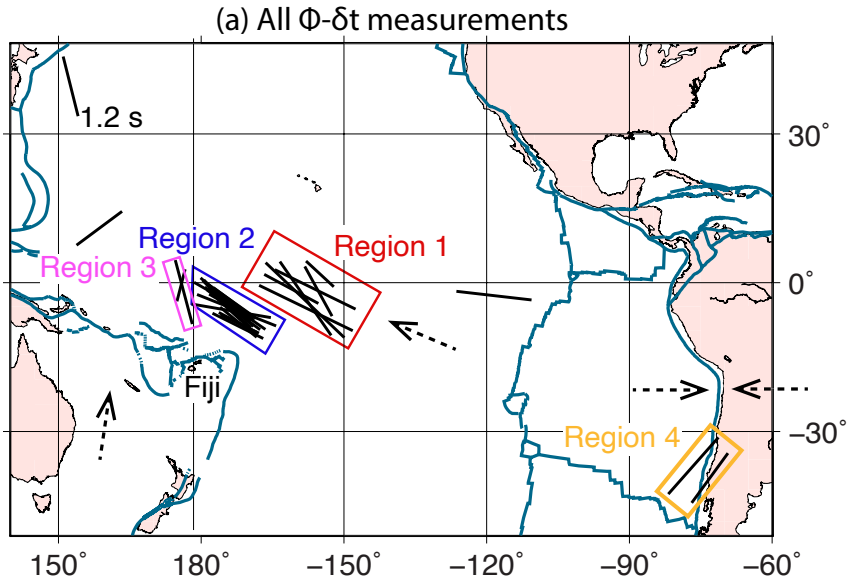

Figure 5: (a) Well-constrained PS ϕ-δt-measurements for null SKS splitting (black sticks), plotted at the PS bounce point in the corresponding reference frame (Section 2). Four regions that show more than one well-constrained measurement are identified (colored boxes). Dashed arrows represent absolute plate motions (DeMets et al., 2010). Plate boundaries (Coffin et al., 1997) are shown by blue lines.

References

Barruol, G., Wüstefeld, A., & Bokelmann, G. (2009). SKS-Splitting-database. *Université de Montpellier, Laboratoire Géosciences*. Retrieved from https://doi.org/10.18715/sks_splitting_database

Becker, T. W. (2012). On recent seismic tomography for the western United States. *Geochemistry, Geophysics, Geosystems, 13*(1), Q01W10. Retrieved from https://doi.org/10.1029/2011GC003977

Becker, T. W., & Lebedev, S. (2021). Dynamics of the upper mantle in light of seismic anisotropy. In *Mantle Convection and Surface Expressions* (pp. 257–282). American Geophysical Union (AGU). Retrieved from https://doi.org/10.1002/9781119528609.ch10

Beyreuther, M., Barsch, R., Krischer, L., Megies, T., Behr, Y., & Wassermann, J. (2010). Obspy: A python toolbox for seismology. *Seismological Research Letters, 81*, 530–533. Retrieved from https://doi.org/10.1111/10.1785/gssrl.81.3.530

Chevrot, S. (2000). Multichannel analysis of shear wave splitting. *Journal of Geophysical Research: Solid Earth, 105*, 21579–21590. Retrieved from https://doi.org/10.1029/2000JB900199

Coffin, M. F., Gahagan, L. M., & Lawver, L. A. (1997). Present-day Plate Boundary Digital Data Compilation. *University of Texas Institute for Geophysics Technical Report No. 174, 199*, 1–6. Retrieved from http://hdl.handle.net/2152/65603

Debayle, E., Dubuffet, F., & Durand, S. (2016). An automatically updated S-wave model of the upper mantle and the depth extent of azimuthal anisotropy. *Geophysical Research Letters, 43*, 674–682. Retrieved from https://doi.org/10.1002/2015GL067329

DeMets, C., Gordon, R. G., & Argus, D. F. (2010). Geologically current plate motions. *Geophysical Journal International, 181*(1), 1–80. Retrieved from https://doi.org/10.1111/j.1365-246X.2009.04491.x

Dziewonski, A. M., & Anderson, D. L. (1981). Preliminary reference Earth model. *Physics of the Earth and Planetary Interiors, 25*, 297–356. Retrieved from https://doi.org/10.1016/0031-9201(81)90046-7

Eakin, C. M., Lithgow-Bertelloni, C., & Dávila, F. M. (2014). Influence of Peruvian flat-subduction dynamics on the evolution of western Amazonia. *Earth and Planetary Science Letters, 404*, 250–260. Retrieved from https://doi.org/10.1016/j.epsl

.2014.07.027

Eddy, C. L., Ekström, G., & Nettles, M. (2022). Three-dimensional seismic anisotropy in the Pacific upper mantle from inversion of a surface-wave dispersion data set. *Geophysical Journal International*, *231*, 355-383. Retrieved from https://doi.org/10.1093/gji/ggac194

Faccenda, M., & Capitanio, F. A. (2012). Development of mantle seismic anisotropy during subduction-induced 3-D flow. *Geophysical Research Letters*, *39*(11), L11305. Retrieved from https://doi.org/10.1029/2012GL051988

Fontaine, F. R., Barruol, G., Tommasi, A., & Bokelmann, G. H. R. (2007). Upper-mantle flow beneath French Polynesia from shear wave splitting. *Geophysical Journal International*, *170*, 1262–1288. Retrieved from https://doi.org/10.1111/j.1365-246X.2007.03475.x

IRIS Transportable Array. (2003). *USArray Transportable Array.* International Federation of Digital Seismograph Networks. Retrieved from https://www.fdsn.org/networks/detail/TA/ doi: 10.7914/SN/TA

Karato, S.-i. (2008). *Deformation of Earth Materials: An Introduction to the Rheology of Solid Earth.* Cambridge University Press. Retrieved from https://doi.org/10.1017/CBO9780511804892

Karato, S.-i., Jung, H., Katayama, I., & Skemer, P. (2008). Geodynamic Significance of Seismic Anisotropy of the Upper Mantle: New Insights from Laboratory Studies. *Annual Review of Earth and Planetary Sciences*, *36*, 59–95. Retrieved from https://doi.org/10.1146/annurev.earth.36.031207.124120

Kneller, E. A., van Keken, P. E., Karato, S.-i., & Park, J. (2005). B-type olivine fabric in the mantle wedge: Insights from high-resolution non-newtonian subduction zone models. *Earth and Planetary Science Letters*, *237*, 781–797. Retrieved from https://doi.org/10.1016/j.epsl.2005.06.049

Lebedev, S., & Van Der Hilst, R. D. (2008). Global upper-mantle tomography with the automated multimode inversion of surface and S-wave forms. *Geophysical Journal International*, *173*, 505-518. Retrieved from https://doi.org/10.1111/j.1365-246X.2008.03721.x

Leng, K., Nissen-Meyer, T., & van Driel, M. (2016). Efficient global wave propagation adapted to 3-D structural complexity: a pseudospectral/spectral-element approach. *Geophysical Journal International*, *207*(3), 1700-1721. Retrieved from

https://doi.org/10.1093/gji/ggw363

Leng, K., Nissen-Meyer, T., van Driel, M., Hosseini, K., & Al-Attar, D. (2019). AxiSEM3D: broad-band seismic wavefields in 3-D global earth models with undulating discontinuities. *Geophysical Journal International*, *217*(3), 2125-2146. Retrieved from https://doi.org/10.1093/gji/ggz092

Link, F., Reiss, M. C., & Rümpker, G. (2022). An automatized XKS-splitting procedure for large data sets: Extension package for SplitRacer and application to the USArray. *Computers & Geosciences*, *158*, 104961. Retrieved from https://doi.org/10.1016/j.cageo.2021.104961

Liu, K., Elsheikh, A., Lemnifi, A., Purevsuren, U., Ray, M., Refayee, H., ... Gao, S. (2014). A uniform database of teleseismic shear wave splitting measurements for the western and central United States. *Geochemistry, Geophysics, Geosystems*, *15*, 2075–2085. Retrieved from https://doi.org/10.1002/2014GC005267

Long, M. D. (2013). Constraints on subduction geodynamics from seismic anisotropy. *Reviews of Geophysics*, *51*(1), 76–112. Retrieved from https://doi.org/10.1002/rog.20008

Long, M. D., & Becker, T. (2010). Mantle dynamics and seismic anisotropy. *Earth and Planetary Science Letters*, *297*, 341-354. Retrieved from https://doi.org/10.1016/j.epsl.2010.06.036

Long, M. D., Biryol, C. B., Eakin, C. M., Beck, S. L., Wagner, L. S., Zandt, G., ... Tavera, H. (2016). Overriding plate, mantle wedge, slab, and subslab contributions to seismic anisotropy beneath the northern Central Andean Plateau. *Geochemistry, Geophysics, Geosystems*, *17*(7), 2556–2575. Retrieved from https://doi.org/10.1002/2016GC006316

Lopes, E., Long, M. D., Karabinos, P., & Aragon, J. C. (2020). SKS Splitting and Upper Mantle Anisotropy Beneath the Southern New England Appalachians: Constraints From the Dense SEISConn Array. *Geochemistry, Geophysics, Geosystems*, *21*, e2020GC009401. Retrieved from https://doi.org/10.1029/2020GC009401

Lynner, C., & Beck, S. L. (2020). Subduction dynamics and structural controls on shear wave splitting along the South American convergent margin. *Journal of South American Earth Sciences*, *104*, 102824. Retrieved from https://doi.org/10.1016/j.jsames.2020.102824

Lynner, C., & Long, M. (2012). Evaluating Contributions to SK(K)S Splitting from Lower

Mantle Anisotropy: A Case Study from Station DBIC, Cote D'Ivoire. *The Bulletin of the Seismological Society of America, 102*, 1030–1040. Retrieved from https://doi.org/10.1785/0120110255

Niu, F., & Perez, A. M. (2004). Seismic anisotropy in the lower mantle: A comparison of waveform splitting of SKS and SKKS. *Geophysical Research Letters, 31*. Retrieved from https://doi.org/10.1029/2004GL021196

Paczkowski, K., Montési, L. G. J., Long, M. D., & Thissen, C. J. (2014). Three-dimensional flow in the subslab mantle. *Geochemistry, Geophysics, Geosystems, 15*, 3989–4008. Retrieved from https://doi.org/10.1002/2014GC005441

Panning, M., & Romanowicz, B. (2006). A three-dimensional radially anisotropic model of shear velocity in the whole mantle. *Geophysical Journal International, 167*, 361–379. Retrieved from https://doi.org/10.1111/j.1365-246X.2006.03100.x

Panning, M. P., & Nolet, G. (2008). Surface wave tomography for azimuthal anisotropy in a strongly reduced parameter space. *Geophysical Journal International, 174*(2), 629–648. Retrieved from https://doi.org/10.1111/j.1365-246X.2008.03833.x

Reiss, M., & Rümpker, G. (2017). SplitRacer: MATLAB Code and GUI for Semiautomated Analysis and Interpretation of Teleseismic Shear-Wave Splitting. *Seismological Research Letters, 88*, 392–409. Retrieved from https://doi.org/10.1785/0220160191

Russo, R., Gallego, A., Comte, D., Mocanu, V., Murdie, R., & VanDecar, J. (2010). Source-side shear wave splitting and upper mantle flow in the Chile Ridge subduction Region. *Geology, 38*, 707–710. Retrieved from https://doi.org/10.1130/G30920.1

Savage, M. K. (1999). Seismic anisotropy and mantle deformation: What have we learned from shear wave splitting? *Reviews of Geophysics, 37*, 65 – 106. Retrieved from https://doi.org/10.1016/10.1029/98RG02075

Silver, P. G. (1996). Seismic Anisotropy beneath the Continents: Probing the Depths of Geology. *Annual Review of Earth and Planetary Sciences, 24*(1), 385 – 432. Retrieved from https://doi.org/10.1146/annurev.earth.24.1.385

Silver, P. G., & Chan, W. W. (1991). Shear wave splitting and subcontinental mantle deformation. *Journal of Geophysical Research: Solid Earth, 96*, 16429–16454. Retrieved from https://doi.org/10.1029/91JB00899

Su, L., & Park, J. (1994). Anisotropy and the splitting of PS waves. *Physics of the Earth and*

Planetary Interiors, *86*, 263–276. Retrieved from https://doi.org/10.1016/0031-9201(94)90125-2

Takeo, A., Kawakatsu, H., Isse, T., Nishida, K., Sugioka, H., Ito, A., ... Suetsugu, D. (2016). Seismic azimuthal anisotropy in the oceanic lithosphere and asthenosphere from broadband surface wave analysis of OBS array records at 60 Ma seafloor. *Journal of Geophysical Research: Solid Earth*, *121*(3), 1927–1947. Retrieved from https://doi.org/10.1002/2015JB012429

Tesoniero, A., Leng, K., D.Long, M., & Nissen-Meyer, T. (2020). Full wave sensitivity of SK(K)S phases to arbitrary anisotropy in the upper and lower mantle. *Geophysical Journal International*, *222*(1), 412 – 435. Retrieved from https://doi.org/10.1093/gji/ggaa171

Trabant, C., Hutko, A. R., Bahavar, M., Karstens, R., Ahern, T., & Aster, R. (2012). Data Products at the IRIS DMC: Stepping Stones for Research and Other Applications. *Seismological Research Letters*, *83*, 846–854. doi: https://doi.org/10.1785/0220120032

Walpole, J., Wookey, J., Masters, G., & Kendall, J. M. (2014). A uniformly processed data set of SKS shear wave splitting measurements: A global investigation of upper mantle anisotropy beneath seismic stations. *Geochemistry, Geophysics, Geosystems*, *15*, 1991–2010. Retrieved from https://doi.org/10.1002/2014GC005278

Walsh, E., Arnold, R., & Savage, M. K. (2013). Silver and Chan revisited. *Journal of Geophysical Research: Solid Earth*, *118*, 5500–5515. Retrieved from https://doi.org/10.1002/jgrb.50386

Wessel, P., & Smith, W. H. F. (1998). New, improved version of generic mapping tools released. *Eos, Transactions American Geophysical Union*, *79*, 579–579. Retrieved from https://doi.org/10.1029/98EO00426

Wolf, J., Creasy, N., Pisconti, A., Long, M. D., & Thomas, C. (2019). An investigation of seismic anisotropy in the lowermost mantle beneath Iceland. *Geophysical Journal International*, *219*(Supplement_1), S152 – S166. Retrieved from https://doi.org/10.1093/gji/ggz312

Wolf, J., Frost, D. A., Long, M. D., Garnero, E., Aderoju, A. O., Creasy, N., & Bozdağ, E. (2023). Observations of Mantle Seismic Anisotropy Using Array Techniques: Shear-Wave Splitting of Beamformed SmKS Phases. *Journal of Geophysical Research: Solid Earth*, *128*, e2022JB025556. Retrieved from https://doi.org/10.1029/2022JB025556

Wolf, J., & Long, M. D. (2022). Slab-driven flow at the base of the mantle beneath the northeastern pacific ocean. *Earth and Planetary Science Letters*, *594*, 117758. Retrieved from https://doi.org/10.1016/j.epsl.2022.117758

Wolf, J., Long, M. D., Creasy, N., & Garnero, E. (2023). On the measurement of Sdiff splitting caused by lowermost mantle anisotropy. *Geophysical Journal International*. Retrieved from https://doi.org/10.1093/gji/ggac490

Wolf, J., Long, M. D., Leng, K., & Nissen-Meyer, T. (2022a). Constraining deep mantle anisotropy with shear wave splitting measurements: Challenges and new measurement strategies. *Geophysical Journal International*, *230*, 507–527. Retrieved from https://doi.org/10.1093/gji/ggac055

Wolf, J., Long, M. D., Leng, K., & Nissen-Meyer, T. (2022b). Sensitivity of SK(K)S and ScS phases to heterogeneous anisotropy in the lowermost mantle from global wavefield simulations. *Geophysical Journal International*, *228*, 366–386. Retrieved from https://doi.org/10.1093/gji/ggab347

Yu, Y., & Park, J. (1993). Upper mantle anisotropy and coupled-mode long-period surface waves. *Geophysical Journal International*, *114*, 473–489. Retrieved from https://doi.org/10.1111/j.1365-246X.1993.tb06981.x

Yuan, K., & Beghein, C. (2014). Three-dimensional variations in Love and Rayleigh wave azimuthal anisotropy for the upper 800km of the mantle. *Journal of Geophysical Research: Solid Earth*, *119*, 3232–3255. Retrieved from https://doi.org/10.1002/2013JB010853

Zhu, H., Yang, J., & Li, X. (2020). Azimuthal Anisotropy of the North American Upper Mantle Based on Full Waveform Inversion. *Journal of Geophysical Research: Solid Earth*, *125*(2), e2019JB018432. Retrieved from https://doi.org/10.1029/2019JB018432